

# Electric Field Modulation of Galvanomagnetic Properties of Mesoscopic Graphite

Yuanbo Zhang, Joshua P. Small, Michael E. S. Amori, and Philip Kim  
*Department of Physics and the Columbia Nanoscale Science and Engineering Center,  
Columbia University, New York, New York 10027*

Electric field effect devices based on mesoscopic graphite are fabricated for galvanomagnetic measurements. Strong modulation of magneto-resistance and Hall resistance as a function of gate voltage is observed as sample thickness approaches the screening length. Electric field dependent Landau level formation is detected from Shubnikov de Haas oscillations in magneto-resistance. The effective mass of electron and hole carriers has been measured from the temperature dependant behavior of these oscillations.

Graphite is a semimetal with highly anisotropic electronic structure featuring nearly compensated low density electrons and holes with very small effective mass [1]. Such an unusual electronic structure is the basis of unique electronic properties of other graphitic materials, such as fullerenes and carbon nanotubes [2], and may lead to novel manifestations in two-dimensional graphene materials. For this reason, electron transport in graphite has recently been the subject of extensive theoretical [3, 4] and experimental [5, 6, 7, 8, 9] investigations. In particular, interesting size dependent galvanomagnetic effect has been observed [10, 11] in thin layers of graphite, with thickness approaching  $\sim 10$  nm. On this mesoscopic length scale, the electrostatic field-effect (EFE) modulation of the charge carrier concentration is expected to be very effective, owing to the low density of nearly compensated carriers in graphite. However, the EFE dependent galvanomagnetic measurements in graphite have not been carried out in previous studies due to the difficulty in obtaining adequate sample geometries.

In this letter, we present results from the magnetoresistance (MR) and Hall resistance measurements in mesoscopic graphite crystallites consisting of as few as  $\sim 35$  atomic layers. Strong modulation of galvanomagnetic transport has been observed as the gate electric field changes. EFE dependent Shubnikov de Haas (SdH) oscillations, signatures of Landau level formation of electrons and holes, have been observed at low temperatures. In addition, the effective mass of electrons and holes are measured by investigating the temperature damping of SdH amplitudes for each type of carriers.

The mesoscopic graphite devices used in this experiment are fabricated using a unique micro-mechanical method. The details of the device fabrication are described elsewhere [12]. In brief, small graphite crystal blocks are extracted from bulk highly oriented pyrolytic graphite (HOPG) using micro-patterning followed by micro-mechanical manipulation. A detached HOPG block is then transferred and fixed onto a micro-machined Si cantilever. By operating an atomic force microscope (AFM) with load on the graphite mounted cantilever, very thin layers of graphite crystallites with lateral size  $\sim 2 \mu\text{m}$  and thickness  $d$  ranging from 10 - 100 nm are

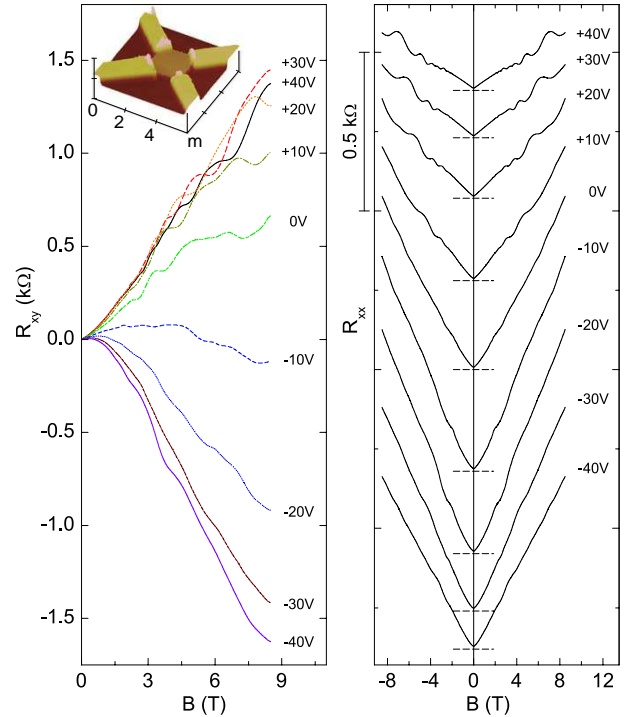


FIG. 1: The inset shows an AFM image of a 12 nm thick mesoscopic graphite sample with four electrodes at the corners for galvanomagnetic measurements. The left and right panel show the Hall resistance ( $R_{xy}$ ) and magneto-resistance ( $R_{xx}$ ) respectively as a function of magnetic field measured at  $T = 1.7$  K in this device. Numbers near each curve indicate the applied gate voltages. In the right panel, curves are shifted for clarity and the dashed lines correspond to the zero lines of each curve.

sheared off onto  $\text{SiO}_2/\text{Si}$  substrate. Multiple metal electrodes (Cr/Au) are then fabricated on the corners, using electron beam lithography (for AFM image of a typical device, see Fig. 1 inset). The degenerately doped silicon substrate serves as a gate electrode with thermally grown silicon oxide (500 nm) acting as the gate dielectric.

Fig. 1 displays the Hall resistance ( $R_{xy}$ ) and the MR ( $R_{xx}$ ) as a function of applied magnetic field,  $B$ , measured in a 12 nm thick graphite sample at temperature  $T = 1.7$  K. The excitation current is kept at  $0.5 \mu\text{A}$  for both  $R_{xy}$  and  $R_{xx}$  measurements. The mag-

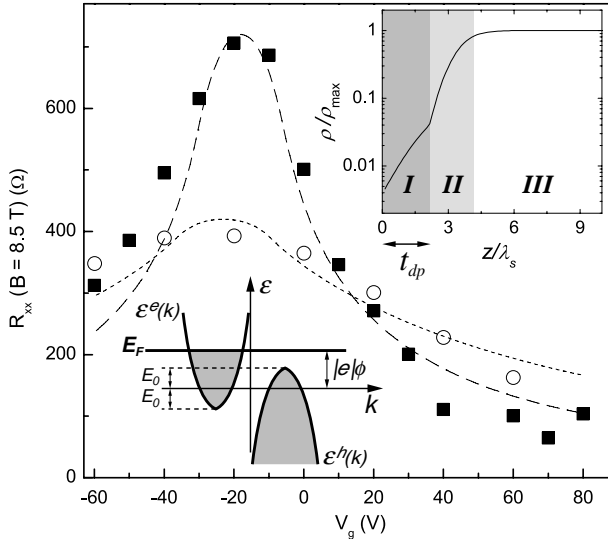


FIG. 2: Magneto-resistance measured in 12 nm (solid square) and 42 nm (open circle) thick sample at various gate voltages. The dashed and dotted lines are fits to a model described in text. The lower inset shows a schematic STB diagram for electron ( $\varepsilon^e(k)$ ) and hole ( $\varepsilon^h(k)$ ) in the presence of electrostatic potential induced by the gate. Upper inset represents the local magneto-resistivity across the sample, assuming  $\phi_0 = 8E_0/|e|$  as an example. Symbols are defined in text.

netic field is applied perpendicularly to the graphite basal plane. Both quantities exhibit oscillatory features on top of smooth backgrounds as  $B$  varies. Near  $V_g \approx 0$  V, the MR and Hall resistance exhibit similar behaviors to those observed in high quality bulk graphite [13]. The “V” shaped MR background is ascribed to the general nature of magnetotransport in materials with coexisting nearly compensated electron and hole carriers [14], while the oscillations on top of the background are related to the SdH effect, the quantum oscillations due to Landau level formation [15]. Remarkably, as we vary the gate voltage,  $V_g$ , the behavior of  $R_{xx}$  and  $R_{xy}$  changes dramatically. The background in the MR is most prominent at  $V_g^{max} \approx -15$  V. As  $V_g$  moves away from this value, the slope of the MR background becomes much smaller. The change of Hall measurement is even more drastic:  $R_{xy}(B)$  changes its sign of overall slope as  $\Delta V_g = V_g - V_g^{max}$  swings from negative to positive values, indicating that  $\Delta V_g$  changes the dominant majority charge carriers from holes to electrons. This is a somewhat surprising result at first sight, since the thickness of the sample (12 nm) is still an order of magnitude larger than the screening length of graphite ( $\lambda_s \approx 0.4$  nm [16]), and thus only relatively small portion of the sample is affected by the gate electric field. We will discuss this point quantitatively below.

The aforementioned EFE in mesoscopic graphite samples is clearly presented by observing  $R_{xx}$  as a function of

gate voltage at a fixed magnetic field. Fig. 2 shows  $R_{xx}$  as a function of  $V_g$  at a large magnetic field ( $B_m = 8.5$  T) for two samples ( $d = 12$  and 42 nm) [17]. As expected from Fig. 1,  $R_{xx}$  has a peak near a gate voltage where  $\Delta V_g \approx 0$ , falling slowly as  $|\Delta V_g|$  becomes large. We found that this gate dependence strongly depends on  $d$ . For the 12 nm sample,  $R_{xx}$  is suppressed to  $\sim 10\%$  of its peak value, while it is still  $\sim 60\%$  for the 42 nm sample at  $\Delta V_g = 80$  V. Such a sensitive dependence of  $R_{xx}(V_g)|_{B_m}$  on  $d$  is indicative of the reduced EFE by screening of induced charge near the sample surface.

In order to elucidate the dependence of  $R_{xx}$  on  $V_g$ , we employ the simple two band (STB) model [18], which has been successful in understanding the MR in graphite [6, 7]. The STB model assumes that the bottom of the electron band and the top of the hole band overlap with a small band overlap  $2E_0$  near the Fermi energy  $E_F$ . The resistivity of a sample,  $\rho$ , in the presence of a magnetic field can be expressed by [14]:

$$\frac{\Delta\rho}{\rho_0} = \frac{4\mu^2 B^2 n_e n_h / (n_e + n_h)^2}{1 + [\mu B (n_e - n_h) / (n_e + n_h)]^2} \quad (1)$$

where  $\rho_0 = \rho(B = 0)$ ,  $\Delta\rho = \rho(B) - \rho_0$ ,  $\mu$  is the average carriers mobility, and  $n_e$  and  $n_h$  are the carrier concentrations of electrons and holes, respectively. Generally,  $\Delta\rho$  varies the most as a function of  $B$  when electrons and holes are nearly compensated (i.e.,  $n_e \approx n_h$ ). From Fig. 2, we infer that this condition is met at  $V_g \approx V_g^{max}$  where the growth of the MR background as a function of  $B$  is strongest in our samples (see the curves for  $V_g = -10$  V and  $V_g = -20$  V in Fig. 1) [19]. As  $\Delta V_g$  increases from zero, the induced charge in the sample screens the gate electric field and the electrostatic potential in the sample is given by  $\phi(z) = \phi_0 e^{-z/\lambda_s}$ , where  $z$  is measured from the interface between the sample and the substrate. The constant  $\phi_0$  can be determined from the electrostatic gate coupling to the sample. By integrating over the induced charge in the sample, we obtain  $\phi_0 = \alpha \Delta V_g$  with the constant  $\alpha^{-1} = 1 + \varepsilon_0(1 - e^{-d/\lambda_s})/\lambda_s C_g$ , where  $C_g$  is the gate capacitance per unit area of the sample and  $\varepsilon_0$  is the vacuum permittivity [12].

We incorporate this local electrostatic potential to the STB model by considering a gradient in  $n_e$  and  $n_h$ . Suppose  $\Delta V_g > 0$ , the local electrostatic potential will pull down the electron and hole bands by  $|e|\phi(z)$  (Fig. 2 lower inset). For a sufficiently large gate voltage, such that  $|e|\phi_0 > E_0$ , the sample can be divided into three regions by introducing a hole depletion depth,  $t_{dp} = \lambda_s \log(|e|\phi_0/E_0)$ : (I)  $0 < z < t_{dp}$ , where  $n_h \simeq 0$ ; (II)  $t_{dp} < z \lesssim t_{dp} + \lambda_s$ , where  $0 < n_h < n_e$ ; and (III)  $z > t_{dp} + \lambda_s$ , where  $n_h \approx n_e$ . In region (I), only electrons participate in the transport, and  $\rho(z)$  increases as  $z$  approaches zero, owing to the electric field induced accumulation of  $n_e$  near the surface. In region (II), the MR is described by Eq. 1, so a steep increase of  $\rho(z)$  is expected as  $n_e - n_h$  becomes small. In region (III),

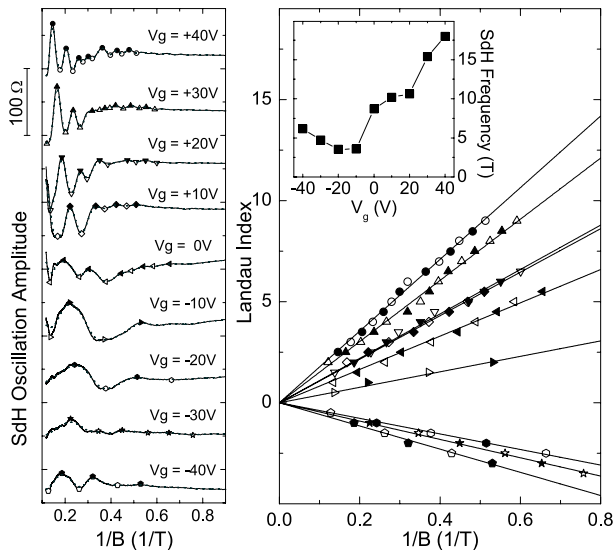


FIG. 3: (a) The SdH Oscillations observed in Fig. 1, after subtraction of smooth backgrounds. Solid (open) symbols correspond to peak (valley) of the oscillations found after passing the curve through a low pass filter (dotted line). Curves are displaced for clarity. (b) Landau plots (see text) obtained from (a). Negative indices are assigned to the hole branch for clarity. Lines are linear fits to each set of points at different  $V_g$ . Inset: the frequency of the SdH oscillations obtained from the slopes of the line fits in (b) as a function of gate voltage.

the gate electric field is completely screened, so  $n_e \approx n_h$  and  $\rho(z) \approx \rho_{max} = R_{xx}(\Delta V_g = 0)d$ . The exact opposite argument works for a sufficiently large negative gate voltage, where electrons are depleted. Note that for small  $|\Delta V_g|$ , where  $|e\phi_0| < E_0$ , region (I) disappears (i.e.,  $t_{dp} = 0$ ). From above discussions, we now build a quantitative model to describe  $\rho(z)$ . According to the STB model  $n_e(\epsilon)$ ,  $n_h(\epsilon) \propto \epsilon^{3/2}$ , where  $\epsilon$  is measured from the bottom of the respective band edge,  $\rho(z)/\rho_{max}$  is obtained from Eq. 1 (Fig. 2 upper inset). Then the resistance of the sample can be evaluated from  $R^{-1} = \int_0^d \rho^{-1}(z)dz$  for fixed  $B$  and  $V_g$ . Following in this way, a reasonable fit is obtained for both 12 nm (dashed line) and 42 nm (dotted line) samples as shown in Fig. 2. In this fit, we use  $E_0 = 15$  meV, a value quoted in [1], and obtain  $C_g = 26$  aF/ $\mu\text{m}^2$  (12 nm sample) and 24 aF/ $\mu\text{m}^2$  (42 nm sample) as a result of the fit. These capacitance values are in reasonable agreement with our previous estimations in a different analysis on the same samples [12]. It is noteworthy that for a large  $V_g$  such that  $|e\phi_0| \gg E_0$ ,  $\rho(z) \ll \rho_{max}$  in region (I), and thus a significant portion of the total current flows in this region. Furthermore, as  $\Delta V_g$  increases,  $t_{dp}$  grows only logarithmically. Even at  $\Delta V_g \approx 100$  V, the largest gate voltage applied,  $t_{dp} \approx 1$  nm, which corresponds to only  $\sim 3$  bottom layers. Therefore, only a few of the bottom layers of the sample are responsible for the observed EFE modulation of the galvanomagnetic transport quantities.

We now turn our attention to the quantum oscillations observed in our mesoscopic graphite samples. The strong EFE modulation of the carrier density in the bottom layers allows us to probe the quantum oscillations in these layers with a continuously tunable carrier concentration. Fig. 3(a) redisplayes the separated SdH oscillations as a function of  $B^{-1}$ , obtained from the MR data shown in Fig. 1 after subtracting out the smooth background. The SdH oscillations indicate the oscillatory density of states at  $E_F$  as a quantized Landau level passes through  $E_F$ . The frequency of SdH oscillations,  $f_s$ , is related to the extremal area of the electron and hole pockets of the Fermi surface by  $f_s = \hbar c A_k^{e,h} / 2\pi |e|$ , where  $A_k^e$  and  $A_k^h$  are the areas of extremal electron and hole pockets, and  $\hbar$  and  $c$  are Plank constant and speed of light respectively [15]. Since  $n_e$  and  $n_h$  are modulated by  $V_g$ , the observed variation of  $f_s$  can be explained by the change of  $A_k^{e,h}$ .

In order to demonstrate the change of  $f_s$  quantitatively, we first locate the major peaks (solid symbols) and valleys (open symbols) in the SdH oscillations after low pass filtering of the data [20]. The value of  $B^{-1}$  for a peak (valley),  $B_m^{-1}$ , is indexed by  $\nu$ , an integer (a half integer) number that corresponds to the Landau level responsible for the particular oscillation. Fig. 3(b) shows that each set of points ( $B_m^{-1}, \nu$ ) at a given  $V_g$  are on a straight line that intercepts the origin, implying that the period of SdH oscillations is regular. From the slope of these lines we obtain  $f_s$  at different  $V_g$  (Fig. 3(b) inset). The obtained  $f_s$ 's are increasing with  $|\Delta V_g|$ . Therefore, we believe that the obtained  $f_s$  corresponds to  $A_k^e$  for  $\Delta V_g > 0$  and to  $A_k^h$  for  $\Delta V_g < 0$ . This conclusion allows us to compare the experimentally observed  $f_s$  with the expected value from the STB model. Assuming the Fermi surface of graphite is described by the overlap of electron and hole bands in STB model,  $A_k^e \propto (\alpha \Delta V_g + E_0)$  and  $A_k^h \propto (-\alpha \Delta V_g + E_0)$ . This relationship leads to  $f_s(|\Delta V_g|)/f_s^0 = 1 + \alpha |\Delta V_g|/E_0$ , where  $f_s^0 = f_s(\Delta V_g = 0)$ . From the values of  $\alpha$  and  $E_0$ , determined separately above, we estimate  $f(\Delta V_g = 50V)/f_0 \approx 4.8$ , which is in reasonable agreement with the experimentally observed ratio 4.3.

Finally, we discuss the temperature dependence of the SdH oscillations. Fig. 4 shows the oscillatory MR at two extreme gate voltages,  $V_g = +40$  V and  $V_g = -60$  V, at various temperatures. At these extreme gate voltages, the transport in the sample is dominated by only one type of carriers in a few bottom layers. Thus, the SdH oscillations in the upper (lower) panel of the figure correspond to electron (hole) Landau levels in the sample. In both cases, the observed SdH oscillation amplitude is gradually damped away as the temperature increases. The temperature dependent SdH oscillation amplitude has been used to extract the effective mass of charge carriers [21]. At a fixed magnetic field, the temperature damping factor of the SdH oscillation amplitude is given

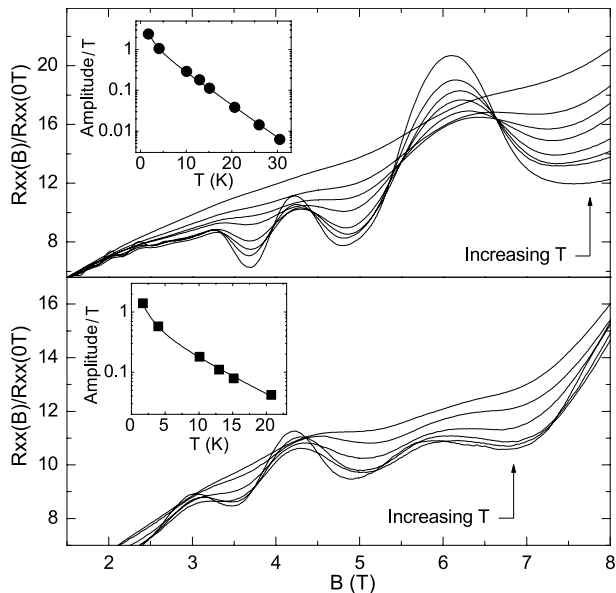


FIG. 4: Normalized magneto-resistance of the sample in Fig 1 at  $V_g = 40$  V (upper panel) and  $V_g = -60$  V (lower panel). For the upper panel data are taken at temperatures 1.7, 4, 10, 13, 15, 20, 25, and 30 K. For the lower panel, data are taken at temperatures 1.7, 4, 10, 13, 15, and 20 K. Insets: SdH oscillation amplitudes divided by temperature,  $T$ , at a fixed magnetic field at above temperatures. The solid lines are fits to a model (see text).

by:

$$R_T = \frac{2\pi^2 k_B T m^* / e\hbar B}{\sinh(2\pi^2 k_B T m^* / e\hbar B)} \quad (2)$$

where  $m^*$  is the effective mass of the carriers. We find that Eq. 2 fits the observed amplitude damping very well (Fig. 4 insets). As a result from the fittings, the effective electron mass  $m_e^* = (0.052 \pm 0.002)m_e$  and hole mass  $m_h^* = (0.038 \pm 0.002)m_e$  are obtained, where  $m_e$  is the bare electron mass. These values agree well with  $0.057m_e$  and  $0.039m_e$ , reported effective mass of electrons and holes in high quality bulk graphite crystal [1].

In summary, we report galvanomagnetic transport in mesoscopic graphite samples consisting of tens of graphene layers. Strong modulation of the Hall resistance as well as the magneto-resistance has been observed as the applied gate voltage changes. The Landau level formation of electron and hole carriers is also tuned by the gate. The unique experimental method discussed here can be applied to other layered materials to investigate novel transport phenomena in unconventional two dimensional systems.

We thank H. L. Stormer, A. Millis and I. Aleiner for helpful discussions. This work is supported primarily by the Nanoscale Science and Engineering Initiative of the

National Science Foundation under NSF Award Number CHE-0117752 and by the New York State Office of Science, Technology, and Academic Research (NYSTAR).

- 
- [1] N. B. Brandt, S. M. Chudinov, and Y. G. Ponomarev, *Semimetals 1: Graphite and its compounds* (North-Holland, 1988).
  - [2] M. S. Dresselhaus, G. Dresselhaus, and P. C. Eklund, *Science of Fullerenes and Carbon Nanotubes* (Academic, 1996).
  - [3] D. V. Khveshchenko, *Phys. Rev.Lett.*, **87**, 246401 (2001); D. V. Khveshchenko, *ibid*, **87**, 246802 (2001).
  - [4] C. D. Spataru, M. A. Cazalilla, A. Rubio, L. X. Benedict, P. M. Echenique, and S. G. Louie, *Phys. Rev. Lett.*, **87**, 246405 (2001).
  - [5] Y. Kopelevish, J. H. S. Torres, R. R. da Silva, F. Mrowka, H. Kempa, and P. Esquinazi, *Phys. Rev.Lett.*, **90**, 156402 (2003).
  - [6] T. Tokumoto, E. Jobiliong, E. S. Choi, Y. Oshima, and J. S. Brooks, *Solid. State. Commun.*, **129**, 599 (2004).
  - [7] X. Du, S. Tsai, D. L. Maslov, and A. F. Hebard, *cond-mat/0404725* (2004).
  - [8] L. M. Viculis, J. J. Jack, and R. B. Kaner, *Science* **299**, 1361 (2003).
  - [9] X. Lu, H. Huang, N. Nemchuk, and R. Ruoff, *Appl. Phys. Lett.* **75**, 193 (1999); X. Lu, M. Yu, H. Huang, and R. Ruoff, *Nanotechnology* **10**, 269 (1999).
  - [10] E. Dujardin, T. Thio, H. Lezec, and T. W. Ebbesen, *Appl. Phys. Lett.* **79**, 2474 (2001).
  - [11] Y. Ohashi, T. Hironaka, T. Kubo, and K. Shiiki, *Tanso* **1997**, 235 (1997); Y. Ohashi, T. Hironaka, T. Kubo, and K. Shiiki, *Tanso* **2000**, 410 (2000).
  - [12] Y. Zhang, J. P. Small, W. Pontius, and P. Kim, submitted for publication.
  - [13] D. E. Soule, *Phys. Rev.* **11**, 698 (1958).
  - [14] I. L. Spain, *Carbon* **17**, 209 (1978).
  - [15] N. W. Ashcroft and N. D. Mermin, *Solid State Physics* (Harcourt College,1976).
  - [16] P. R. Visscher and L. M. Falicov, *Phys. Rev. B* **3**, 2541 (1971).
  - [17] We measured 6 mesoscopic graphite samples with the thickness ranging 12 - 95 nm. Similar result was found the sample with the similar geometry.
  - [18] For an extensive summary see, for example, B. T. Kelly *Physics of Graphite* (Applied Science,1981), pp285.
  - [19]  $\Delta R_{xx}(H)/R_{xx}$  increases rather linearly than quadratic increase as predicted from the STB model. Similar behavior has been observed other bulk graphite samples (see, for e.g., Y. Kaburagi and Y. Hishiyama, *Carbon* **33**, 1505 (1995) and reference therein.). This deviation is, however, not essential in our argument in this paper.
  - [20] In principle, we expect to see two distinct oscillation periods caused by electrons and holes in graphite. However, due to the finite lateral size of sample ( $L = 2 \mu\text{m}$ ), only the cyclotron orbits whose diameters are much smaller than  $L$  contribute most in the observed SdH oscillations.
  - [21] D. Shoenberg, *Magnetic oscillations in metals*, (Cambridge University Press, 1984).